Selective Growth of Metal Tips onto Semiconductor Quantum Rods and Tetrapods

Taleb Mokari *et al.*

Science **304**, 1787 (2004);
DOI: 10.1126/science.1097830

Science (print ISSN 0036-8075; online ISSN 1095-9203) is published weekly, except the last week in December, by the American Association for the Advancement of Science, 1200 New York Avenue NW, Washington, DC 20005.

30. W. Schultz, *Curr. Opin. Neurobiol.* **14**, 139 (2004).
31. D. J. Barraclough, M. L. Conroy, D. Lee, *Nature Neurosci.* **7**, 404 (2004).
32. M. C. Dorris, P. W. Glimcher, *Soc. Neurosci. Abstr.* **767**, 1 (2003).
33. J. W. Bisley, M. E. Goldberg, *Science* **299**, 81 (2003).
34. C. Koch, S. Ullman, *Hum. Neurobiol.* **4**, 219 (1985).
35. L. Itti, C. Koch, *Nature Rev. Neurosci.* **2**, 194 (2001).
36. R. J. Herrnstein, W. Vaughan, in *Limits to Action: The Allocation of Individual Behavior*, J. E. R. Staddon, Ed. (Academic Press, New York, 1980), pp. 143–176.
37. R. J. Herrnstein, D. Prelec, *J. Econ. Perspect.* **5**, 137 (1991).
38. M. Davison, W. M. Baum, *J. Exp. Anal. Behav.* **74**, 1 (2000).
39. C. B. Harley, *J. Theor. Biol.* **89**, 611 (1981).
40. We thank C. R. Gallistel for advice in the planning of these experiments; W. Bair and H. S. Seung for contributions to data analysis; A. E. Rorie for discussions; S. Rosenbaum for animal training; and J. M. Nichols and M. Cohen for comments on an early version of this manuscript. Supported by the National Eye Institute and the Howard Hughes Medical Institute. L.P.S. and G.S.C. received additional support from Stanford Graduate Fellowships.

Supporting Online Material
www.sciencemag.org/cgi/content/full/304/5678/1782/DC1
Materials and Methods
Fig. S1
References and Notes

16 December 2003; accepted 22 April 2004

REPORTS

Selective Growth of Metal Tips onto Semiconductor Quantum Rods and Tetrapods

Taleb Mokari,[1,2] Eli Rothenberg,[1,2] Inna Popov,[2] Ronny Costi,[1,2] Uri Banin[1,2]*

We show the anisotropic selective growth of gold tips onto semiconductor (cadmium selenide) nanorods and tetrapods by a simple reaction. The size of the gold tips can be controlled by the concentration of the starting materials. The new nanostructures display modified optical properties caused by the strong coupling between the gold and semiconductor parts. The gold tips show increased conductivity as well as selective chemical affinity for forming self-assembled chains of rods. Such gold-tipped nanostructures provide natural contact points for self-assembly and for electrical devices and can solve the difficult problem of contacting colloidal nanorods and tetrapods to the external world.

Anisotropic growth of nanomaterials has led to the development of complex and diverse nanostructures such as rods (*1*, *2*), tetrapods (*3*), prisms (*4*), cubes (*5*), and additional shapes (*6*, *7*). These architectures display new properties and enrich the selection of nano–building blocks for electrical, optical, and sensorial device construction. New functionality, such as emissive or rectifying junctions, is introduced into the nanostructure by anisotropic growth with compositional variations. This has been realized by growing semiconductor heterostructures such as p-n junctions and material junctions (e.g., GaAs/GaP) in nanowires (*8*, *9*). In the case of colloidal nanocrystals, growth of a dot-rod structure composed of two different semiconductors and other complex branched structures was achieved (*10*). In these examples, anisotropic growth was performed with the same material type (semiconductor). Here we report the selective anisotropic growth of two different material systems, a metal onto a semiconductor. We developed a simple method for the selective growth of gold dots onto the tips of colloidal semiconductor nanorods and tetrapods. This combination provides new functionalities to the nanostructures, the most important of which is the formation of natural anchor points that can serve as a recognition element for directed self-assembly and for wiring them onto electrical circuitry.

This advancement has direct relevance to the problem of contact reproducibility and contact resistance that has hindered the study of conductance in nanostructures. Recently there have been reports of good connectivity for micrometer-long quasi–one-dimensional structures such as nanotubes and nanowires (*11*–*13*). However, wiring of the shorter colloidal semiconductor rods and tetrapods studied here, with arm lengths of less than 100 nm, has long been an open issue. The use of bifunctional organic ligands, primarily dithiols, as contacting ligands—as used in scanning tunneling microscopy studies (*14*) and in transport measurements (*15*)—creates a tunneling barrier, and transport is often dominated by the contact resistances. The use of DNA-based assembly for creating functional circuitry (*16*, *17*) also requires selective anchor points for the directed assembly of nanostructures (*18*). The Au tips are natural recognition elements for this task as well as for creating complex self-assembled architectures with semiconductor rods and tetrapods in solution (*19*) and onto substrates.

We prepared CdSe rods and tetrapods of different dimensions by high-temperature pyrolysis of suitable precursors in a coordinating solvent containing a mixture of trioctylphosphineoxide and phosphonic acids (*1*, *20*, *21*). We dissolved $AuCl_3$ in toluene with the addition of dodecyldimethylammonium bromide (DDAB) and dodecylamine. For growth of Au tips, we mixed this solution at room temperature with a toluene solution of the colloidal-grown CdSe nanorods or tetrapods. After the reaction, the quantum rods were precipitated by addition of methanol and separated by centrifugation. The purified product could then be redissolved in toluene for further study (*22*).

Figure 1 presents transmission electron microscopy (TEM) images showing growth of Au onto CdSe quantum rods of dimensions 29 × 4 nm (length × diameter); the procedure involved gradual addition of larger amounts of Au precursors (see Table 1 for details). Selective Au growth onto the rod tips (Fig. 1, B to D) is clearly identified as the appearance of points with enhanced contrast. The rods now appear as "nano-dumbbells." Moreover, by controlling the amount of initial Au precursor, it is possible to control the size of the Au tips on the nano-dumbbell edges, from ~2.2 nm (Fig. 1B) to ~2.9 nm (Fig. 1C) to ~4.0 nm (Fig. 1D) (see Table 1). The procedure clearly leads to the growth of

Table 1. Details for Au growth on 29 × 4 nm rods as shown in Fig. 1, with average dimensions (full histograms are shown in fig. S1).

Sample	Nanocrystals (mg)	Dodecylamine (mg)	DDAB (mg)	$AuCl_3$ (mg)	Rod size (L × D, nm)	Gold ball size (nm)
1	—	—	—	—	29 × 4	(original rod)
2	10	40	25	4	25.6 × 3.3	2.22
3	10	90	50	8	23.9 × 3.4	2.9
4	10	160	100	13.5	20.8 × 3.2	4

[1]Institute of Chemistry, Farkas Center for Light-Induced Processes, [2]Center for Nanoscience and Nanotechnology, Hebrew University of Jerusalem, Jerusalem 91904, Israel.

*To whom correspondence should be addressed. E-mail: banin@chem.ch.huji.ac.il

natural contact points on the tips of the rods.

An additional observation from the analysis of ~200 particles per sample is that the overall rod length becomes shorter upon Au growth, and there is also a decrease in the average diameter of the rods (Table 1; see fig. S1 for sizing histograms). Control experiments with DDAB and dodecylamine, but without $AuCl_3$, also showed a decrease in rod dimensions (table S1). Hence, reduction of rod size is related to dissolution of rods in the presence of DDAB and not to the Au growth.

Figure 2A shows energy-dispersive x-ray (EDX) spectroscopy of a micrometer area with rods after growth; the appearance of Au in the goldenized and purified rod sample is clear. The powder x-ray diffraction pattern for the 29 × 4 nm rod sample comparing the rods before and after gold growth is shown in Fig. 2B. The appearance of the Au (111), (200), and (220) peaks after Au growth provides evidence that crystalline Au is formed on the tips.

Further evidence for Au growth onto single rods is provided by HRTEM (high-resolution TEM) studies of the nano-dumbbells. Figure 2C shows a HRTEM image of a single rod after gold treatment. The lattice image for the rod part composed of CdSe corresponds to growth of rods along the CdSe ⟨001⟩ axis, consistent with the earlier studies (*1*, *20*, *21*). The Au is again discerned as the region at the edge with enhanced contrast; the gold lattice is also shown in Fig. 2D. Because of the difference in contrast of CdSe and Au and the orientation of the rod relative to the electron beam, it is difficult to clearly observe both lattice images simultaneously, but under different imaging conditions we could verify the presence of the CdSe lattice in the center (Fig. 2C) and the Au lattice in the edges (Fig. 2D). The detailed Au-CdSe interface is difficult to study. Our analysis on ~15 rods shows different relative angles for the Au and CdSe lattice, implying that the growth can take place in different forms. However, at the Au-CdSe interface, we can expect Au-Se bonds analogous to the known AuSe material (*23*). This means that the interface is formed with covalent chemical bonds between the metal and the semiconductor and hence can be expected to provide good electrical connectivity.

The method for selective Au growth could be easily expanded and applied to rods of arbitrary dimensions (fig. S2). A remarkable result is obtained for Au growth on CdSe tetrapods, as can be seen in Fig. 3A (showing several tetrapods) and Fig. 3B (showing an enlargement of one tetrapod). Growth occurs selectively on all four tips of the tetrapods, leading a tetrahedral arrangement for the Au tips and once again providing natural contact points for self-assembly of novel structures and for electrical connections.

We have grown metal tips onto CdSe/ZnS core/shell nanorods (29 × 4 nm rods with 2-monolayer ZnS shell) with initial emission quantum yield of 2%. Treatment of these rods with DDAB and dodecylamine without Au led to an increased quantum yield of 4%, likely because of the effect of the excess amine. Au tips with sizes from ~2 to 4.5 nm were grown onto the rods. Absorption and photoluminescence (PL) measurements were carried out to study the effect of Au growth on the rod optical properties (Fig. 4). Absorption spectra (Fig. 4A) for the small Au tips on

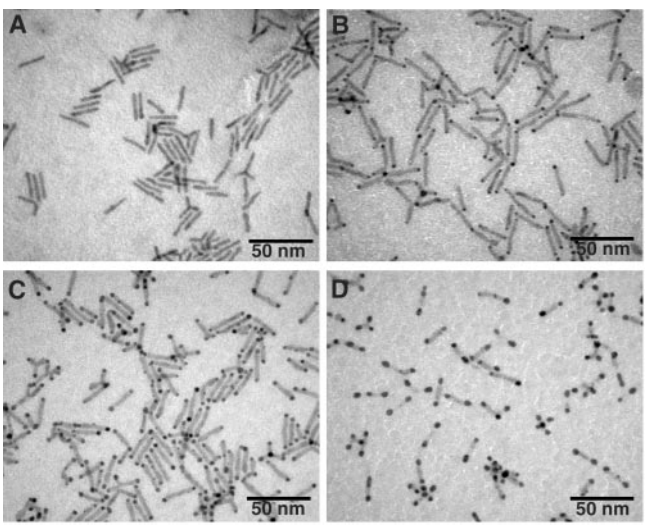

Fig. 1. TEM images showing controlled growth of Au onto the tips of CdSe quantum rods. (**A**) Original rod sample, 29 × 4 nm. (**B** to **D**) Rod samples 2, 3, and 4, respectively (Table 1) after Au treatment using gradually increased $AuCl_3$ concentrations; increased Au tip sizes are visible.

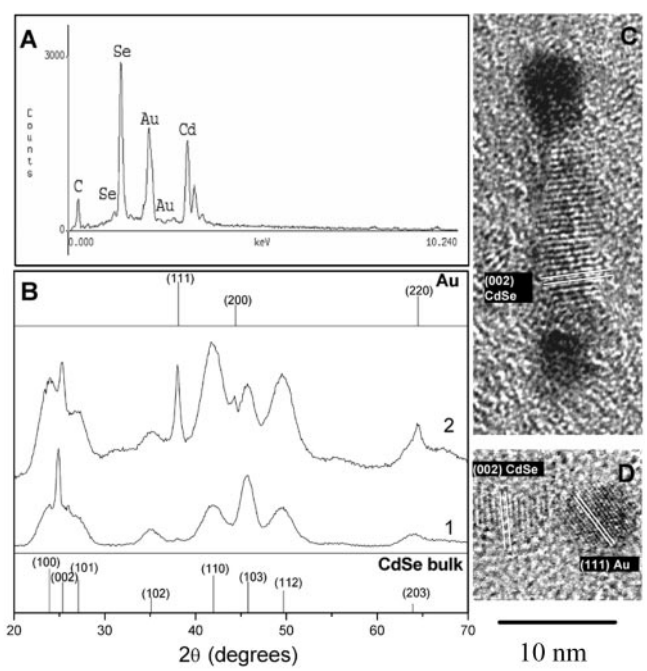

Fig. 2. Structural and chemical characterization of CdSe-Au nano-dumbbells. (**A**) EDX spectrum of the goldenized CdSe rod sample. The relative atom percentage of Au:Cd:Se was 18%:42%:40%. (**B**) Powder x-ray diffraction comparing CdSe rods before (1) and after (2) Au growth. Bulk CdSe and Au peaks are marked. Crystalline Au clearly appears after the growth process. Intensity redistribution in favor of the (002) CdSe peak in the original rods is a result of partial alignment in the deposited rod sample, in which rods grow along ⟨001⟩. (**C** and **D**) HRTEM images of a single nano-dumbbell and a nano-dumbbell tip, respectively. The CdSe lattice for the rod in the center and Au tips at the rod edges can be identified, as marked.

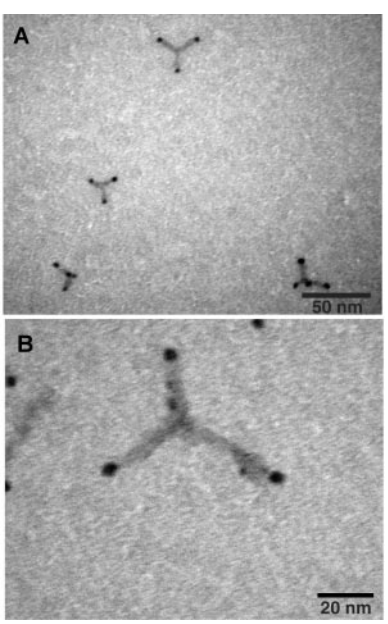

Fig. 3. Au growth on tips of CdSe tetrapods: a general view (**A**) and higher magnification for one tetrapod (**B**).

the rods still show the excitonic structure, but with increased absorbance in the visible spectrum and the appearance of a tail to the red side of the particle gap. Upon increased Au size, the features of the absorption of the rods are washed out and the tail to the red side becomes more prominent. The spectra should contain, in principle, contributions from the semiconductor part and the plasmon resonance associated with the Au tips. However, we emphasize that attempts to add spectra of the rod template and Au nanocrystals did not reproduce the observed absorption, and we conclude that the spectra are not a simple sum of both components. Instead, these results reflect the modified electronic structure of the Au-rod nano-dumbbell system. The strong mixing of the semiconductor and metal electronic states leads to modified density of states exhibiting broadened levels and a reduced band gap.

The strong coupling of the Au is also observed for the PL (Fig. 4B), which undergoes considerable quenching with increased Au ball size, by a factor of ~100 for the smaller Au balls (~2 nm) and increasing to a factor of ~500 for the large Au balls (~4.5 nm). Quenching of the emission by the metal tips is expected via the new nonradiative pathways created by the proximity of metal, likely leading to electron transfer to the Au. This behavior resembles the superquenching effect by highly efficient energy transfer from conjugated polymers to gold nanoparticles (*24*). Moreover, a systematic dependence of quenching on Au size is seen, as shown in the Stern-Volmer type plot (inset, Fig. 4B), resembling the observation in the Au-polymer case (*25*). Both absorption and emission spectra exemplify the large effect of the Au on the semiconductor rod properties in this new system, providing further evidence of the strong bonding of the Au to the CdSe rod.

The role to be played by the Au tips as contact points for wiring the rods is exemplified by conductive atomic force microscopy (C-AFM) measurements carried out on goldenized 60 × 6 nm rods (TEM in fig. S2F). Rods were deposited onto a conducting highly ordered pyrolitic graphite substrate and embedded in a thin layer of poly(methyl methacrylate) (PMMA) to avoid dragging by the tip, as reported earlier for regular rods (*26*). The current image of a single rod measured by this method reveals that already at a bias of 1.5 to 2 V, small tunneling current is flowing through the tips composed of Au, whereas the central part of the rod consisting of the semiconductor is nonconductive at these conditions (Fig. 4C) (fig. S3). The small tunneling current is determined by the tunneling barriers at tip-nanocrystal and nanocrystal-substrate junctions, dominated primarily by the PMMA. This measurement reveals the notably higher conductance of the Au tips, which would be critical for their use as electrical contact points.

The selective tip growth of Au onto the rods and tetrapods not only has potential importance for enabling electrical connectivity and new paths for self-assembly for such nanostructures; it is also an interesting chemical reaction route with clear selectivity and anisotropic character. The reaction mechanism for the gold growth entails a reduction of Au. TEM examination of the Au solution with DDAB and dodecylamine shows formation of Au particles (fig. S4). This is consistent with earlier reports on the formation of Au particles with amine precursors (*27*) and on Ag nanoparticle formation under mild conditions (*28*). The further role of dodecylamine is revealed from experiments carried out without amine. In this case, considerable aggregation of the CdSe rods was seen (fig. S5). Dodecylamine is known to stabilize the rods and prevent aggregation (*29*). Additionally, without the amine, growth of Au on rods was not initially apparent; only after irradiation under the TEM beam did we observe some Au growth (fig. S5).

The most compelling aspect of the procedure reported here is its specificity leading to selective tip growth. This is assigned to the preferential adsorption of the Au complex onto the rod tips. The tips are more reactive because of the increased surface energy and also possibly because of imperfect passivation of the ligands on these faces, which also leads to preferential growth along the ⟨001⟩ axis of CdSe rods (*1*, *20*). Once Au nucleates on the edge, it is preferential for additional Au to adhere and grow on that seed. This claim of favored growth on the seed gains support from controlling the Au tip size on the rods by using increased concentration of Au in the gold solution, as was shown in Fig. 1. Moreover, early Au growth as shown in Fig. 1B reveals that in some rods preferential early growth occurs on one tip, in agreement with the surfactant-controlled growth model suggested for CdSe rods (*1*, *20*, *21*). From the viewpoint of chemical reactivity, the asymmetry in reaction to selectively occur at the tips versus the rest of the nanostructure is fascinating.

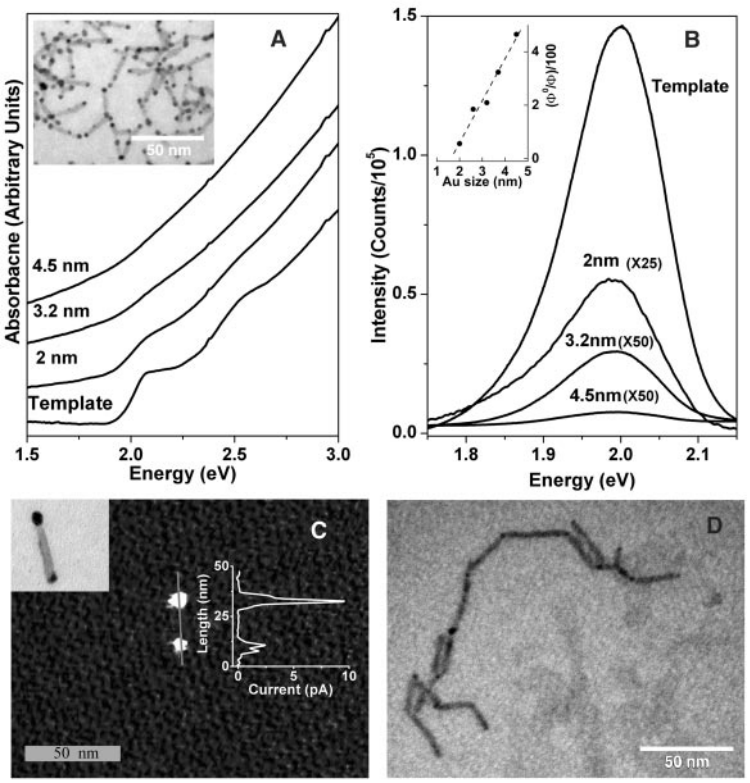

Fig. 4. Novel properties of nano-dumbbells. (**A** and **B**) Optical spectra for CdSe-ZnS core-shell nanorod sample with varied Au tip size compared to the original rod template. (A) Absorption spectra; Au tip size is indicated. Spectra are offset vertically for clarity. Inset shows TEM image of the sample after Au growth. (B) Photoluminescence spectra; Au tip size is indicated for each trace. Traces were multiplied by 25, 50, and 50 for the 2-nm, 3.2-nm, and 4.5-nm Au tips, respectively, for clarity. Inset shows a plot of relative PL yield for template (Φ^0) over Au rod (Φ) versus Au ball size. Measurements were performed for rod solutions in a sealed cuvette under Ar using the 454-nm line of an Ar-ion laser with intensity of 100 mW. Fluorescence was collected under identical conditions for all solutions in a right-angle configuration with a spectrograph/charge-coupled device setup, with integration time of 500 ms. (**C**) C-AFM current image of single nano-dumbbell measured at a sample bias of 2 V. Higher conductance through the Au tips is observed, as seen also by the current cut taken along the rod (along plotted line). In the inset, a TEM image with the same scale of an Au rod is shown for comparison. (**D**) TEM of a self-assembled chain of nano-dumbbells (29 × 4 nm) formed by adding hexane dithiol bifunctional linker molecules.

In some cases we can identify Au growth on branching and defect points, but at a slower rate relative to the distinctive tip growth discussed above. Weak, dark Au spots also appear in some positions other than the tips of the long rods (fig. S2F) and tetrapods (Fig. 3B). This growth can be controlled by the amounts of Au added to the rods. At such defect points, such as points where the diameter of the structure changes, there is also increased reactivity as a result of the imperfect chemical bonding and increased surface energy. This leads to Au adhesion and growth, in agreement with the mechanism for tip growth. We emphasize that the tip growth occurs more readily and rapidly than growth on the defects and hence can be controlled to achieve contact points.

To demonstrate the use of such contact points as recognition elements for self-assembly, we show the self-assembly of goldenized rods to form chains via linking through the gold tips. A simple approach was taken where hexane dithiol was added to a solution of rods as a bifunctional ligand. The thiol group binds strongly and preferentially to the Au tips, and the bifunctional ligand thus allows for preferential linking of rods in a head-to-tail arrangement forming chains of rods (Fig. 4D), whereas the usual preference for rod aggregation is side to side (fig. S6). This kind of self-assembly strategy can be used to assemble the goldenized rods onto electrode structures or onto DNA circuitry.

References and Notes

1. X. G. Peng *et al.*, *Nature* **404**, 59 (2000).
2. S. H. Kan *et al.*, *Nature Mater.* **2**, 155 (2003).
3. L. Manna *et al.*, *Nature Mater.* **2**, 382 (2003).
4. R. Jin *et al.*, *Science* **294**, 1901 (2001).
5. F. Dumestre *et al.*, *Science* **303**, 821 (2004).
6. Z. Tang *et al.*, *Science* **297**, 237 (2002).
7. J. Goldberger *et al.*, *Nature* **422**, 599 (2003).
8. M. S. Gudiksen *et al.*, *Nature* **415**, 617 (2002).
9. Y. Wu, R. Fan, P. Yang, *Nano Lett.* **2**, 83 (2002).
10. D. V. Talapin *et al.*, *Nano Lett.* **3**, 1677 (2003).
11. Y. Cui, C. M. Lieber, *Science* **291**, 851 (2001).
12. S. Heinze *et al.*, *Phys. Rev. Lett.* **89**, 106801 (2002).
13. A. Javey *et al.*, *Nature* **424**, 654 (2003).
14. U. Banin, O. Millo, *Annu. Rev. Phys. Chem.* **54**, 465 (2003).
15. D. L. Klein *et al.*, *Nature* **389**, 699 (1997).
16. E. Braun *et al.*, *Nature* **391**, 775 (1998).
17. H. Yan *et al.*, *Science* **301**, 1882 (2003).
18. K. Keren *et al.*, *Science* **302**, 1380 (2003).
19. K. K. Caswell *et al.*, *J. Am. Chem. Soc.* **123**, 13914 (2003).
20. L. Manna *et al.*, *J. Am. Chem. Soc.* **122**, 12700 (2000).
21. Z. A. Peng, X. Peng, *J. Am. Chem. Soc.* **123**, 1389 (2001).
22. See supporting data on *Science* Online.
23. J. E. Cretier, G. A. Wiegers, *Mater. Res. Bull.* **8**, 1427 (1973).
24. C. Fan *et al.*, *Proc. Natl. Acad. Sci. U.S.A.* **100**, 6297 (2003).
25. R. M. Jones *et al.*, *Proc. Natl. Acad. Sci. U.S.A.* **98**, 14769 (2001).
26. E. Nahum *et al.*, *Nano Lett.* **4**, 103 (2004).
27. S. Gomez *et al.*, *Chem. Comm.* **2000**, 1945 (2000).
28. M. Yamamoto, M. Nakamoto, *J. Mater. Chem.* **13**, 2064 (2003).
29. T. Mokari, U. Banin, *Chem. Mater.* **15**, 3955 (2003).

30. Supported by the U.S.-Israel Binational Science Foundation. We thank Y. Cui, A. P. Alivisatos, and P. Yang for helpful discussions.

Supporting Online Material

www.sciencemag.org/cgi/content/full/304/5678/1787/DC1
Materials and Methods
SOM Text
Figs. S1 to S6
Table S1

12 March 2004; accepted 6 May 2004

Ultrahigh-Resolution Spin-Echo Measurement of Surface Potential Energy Landscapes

Andrew P. Jardine,* Shechar Dworski, Peter Fouquet,† Gil Alexandrowicz, David J. Riley, Gabriel Y. H. Lee, John Ellis, William Allison

We demonstrate two approaches that use the recently developed helium spin-echo technique to measure surface potential energy landscapes. For helium–lithium fluoride (100), we use the selective adsorption phenomenon to obtain the complete experimental band structure of atoms in a corrugated surface potential. For carbon monoxide–copper (001), we measure the diffusion-induced energy broadening in the scattered helium beam and extract properties of the adsorbate-substrate potential. The measurements are made possible by the resolution of our new spectrometer, which improves on existing resolution by three orders of magnitude. We show that it is possible to produce benchmark energy landscapes to assist evaluation and development of first-principles theory in the problematic van der Waals/weak chemisorption regime.

First-principle calculations provide powerful tools for assisting in the design of new catalysts for the chemical industry and helping elucidate critical steps in semiconductor device growth and development (*1*). However, these methods still have several limitations, the most important being that they do not include van der Waals forces and that their absolute accuracy (as demonstrated by variations in the results given with different functionals) is limited to ~0.1 eV (*1*). For weak chemisorption, so important in catalysis, and for soft condensed matter simulations, these represent real limitations. One important issue in the further development of calculational methods is the need for benchmark experimental data to evaluate theoretical predictions. Often all that is available are a few, albeit well-defined, data points—a binding energy or the temperature of a phase transition. We describe techniques that can deliver detailed information on a whole energy landscape for atom/molecule-surface systems produced by observing the way an atomic species moves around in the potential at the surface.

Thermal energy atom scattering is an inert, completely nondestructive, and exclusively surface-sensitive probe (*2*–*4*). Helium "spin-echo" techniques (*5*) provide two methods in which the energy landscape can be explored. The most general method is through quasi-elastic helium atom scattering (*6*) (QHAS) from a moving adsorbate. In this method, the small, Doppler-like energy broadening induced in a probe of He atoms gives insights into the adsorbate dynamics and hence the energy landscape in which the adsorbate moves. Because QHAS measures on the angström length and picosecond time scales that are characteristic of atomistic dynamics, it provides a level of detail and a scope of measurement (*2*, *6*) that are not available with any other technique. Alternatively, for certain systems, it is possible to obtain a direct measure of the bound states of the probe atoms within the attractive part of the surface potential through the phenomenon of selective adsorption resonance (SAR) (*3*, *4*). We apply these techniques to two seminal surface systems: CO-Cu (001) and He-LiF (100).

Our measurements take advantage of the resolution of a new spectrometer to analyze the energies in a scattered He beam with a much higher resolution than has previously been possible. In conventional He-scattering instruments, energy resolution is achieved by chopping the beam into short packets. These packets spread out along the beam line before their times of flight are measured up to a particular detection point (*3*). Such instruments are limited by the achievable level of monochromaticity within the incident beam and the size of the active detection region.

Spin-echo instruments circumvent such limitations by using nuclear spin-precession to achieve much greater energy resolution. The technique was originally applied to neutron scattering (*7*) and more recently to molecular beams (*5*, *8*), although at energies below the diffraction threshold, where it is impossible to obtain the data reported here. A beam energy sufficiently high to excite surface processes is essential, but high beam energies make high resolution more difficult to achieve. Our instrument can fulfill both the beam energy and resolution criteria.

A collimated beam of ^{3}He atoms was produced in a supersonic free jet source (*9*).

Cavendish Laboratory, University of Cambridge, Madingley Road, Cambridge CB3 0HE, UK.

*To whom correspondence should be addressed. E-mail: apj24@cam.ac.uk

†Present address: Institut Laue Langevin, 6 Rue Jules Horowitz, BP 156, 38042 Grenoble Cedex 9, France.